



**HAL**  
open science

## Bio-inspired apatite particles limit skin penetration of drugs for dermatology applications

Maëla Choimet, Audrey Tourrette, Olivier Marsan, Giovanna Rassu,  
Christophe Drouet

### ► To cite this version:

Maëla Choimet, Audrey Tourrette, Olivier Marsan, Giovanna Rassu, Christophe Drouet. Bio-inspired apatite particles limit skin penetration of drugs for dermatology applications. *Acta Biomaterialia*, 2020, 111, pp.418-428. 10.1016/j.actbio.2020.05.010 . hal-03095508

**HAL Id: hal-03095508**

**<https://hal.science/hal-03095508>**

Submitted on 4 Jan 2021

**HAL** is a multi-disciplinary open access archive for the deposit and dissemination of scientific research documents, whether they are published or not. The documents may come from teaching and research institutions in France or abroad, or from public or private research centers.

L'archive ouverte pluridisciplinaire **HAL**, est destinée au dépôt et à la diffusion de documents scientifiques de niveau recherche, publiés ou non, émanant des établissements d'enseignement et de recherche français ou étrangers, des laboratoires publics ou privés.

## **Bio-inspired apatite particles limit skin penetration of drugs for dermatology applications**

Maëla Choimet<sup>1,2,3</sup>, Audrey Tourrette<sup>2,\*</sup>, Olivier Marsan<sup>1</sup>, Giovanna Rassu<sup>4</sup>, Christophe Drouet<sup>1,\*</sup>

<sup>1</sup>CIRIMAT Carnot Institute, UMR CNRS/INPT/UPS 5085, University of Toulouse, Ensiacet, 4 allée E. Monso, 31030 Toulouse cedex 4, France

<sup>2</sup>CIRIMAT Carnot Institute, UMR CNRS/INPT/UPS 5085, University of Toulouse, Faculté des Sciences Pharmaceutiques, 35 Chemin des Maraîchers, 31400 Toulouse, France

<sup>3</sup>*Present address:* SEPPIC – Air Liquide Healthcare, 127 chemin de la Poudrerie, 81105 Castres, France

<sup>4</sup>Department of Chemistry and Pharmacy, University of Sassari, Via Muroni 23/a, 07100 Sassari, Italy

\*Corresponding Authors:

Dr. Christophe Drouet (ORCID # 0000-0002-8471-8719 ; SCOPUS Author ID # 7004734485)

CIRIMAT, Ensiacet,

4 allée Emile Monso,

31030 Toulouse cedex 4, France

e-mail: [christophe.drouet@cirimat.fr](mailto:christophe.drouet@cirimat.fr)

Dr. Audrey Tourrette-Diallo (ResearchID # R-2763-2017)

CIRIMAT, Faculté des Sciences Pharmaceutiques, Université Paul Sabatier

Allée des Maraichers,

31029 Toulouse cedex 4, France

e-mail: [audrey.tourrette@univ-tlse3.fr](mailto:audrey.tourrette@univ-tlse3.fr)

## **Abstract**

Most treatments of skin pathologies involve local administration of active agents. One issue can however be the partial transcutaneous diffusion of the drug to blood circulation, leading to undesirable effects. In this work, the original use of submicron mineral particles based on bio-inspired calcium phosphate apatite was explored for the first time as drug carriers for favoring topical delivery. The permeation of a model drug across synthetic and biological membranes was investigated in both static and dynamic conditions. Our data show that adsorption of the drug on the apatite particles surface drastically limits its permeation, with lower effective diffusion coefficients ( $P_{\text{eff}}$ ) and smaller total released amounts. The retention of the apatite colloidal particles on porcine ear skin explants surface was demonstrated by combining histological observations and Raman confocal microscopy. All results converge to show that association of the drug to apatite particles favors skin surface effects. These findings point to the relevance of mineral-based particles as drug carriers for local delivery to the skin, and open the way to novel applications of bio-inspired apatites in dermatology.

## **Statement of significance**

Calcium phosphates (CaP) are major biomaterials in orthopedics and dentistry. Their resemblance to bone mineral allows new applications beyond bone repair, e.g. in nanomedicine. In 2018, a 14-page detailed review (M. Epple, *Acta Biomaterialia* 77 (2018) 1–14) provided clear facts in favor of the non-toxicity of nanosized CaP as an answer to discussions from EU and US study groups, thus clarifying the path to novel applications of nano CaP. In the present paper, bio-inspired apatite nanoparticles are used for the first time as drug carriers for dermatology for drastically limiting drug transcutaneous permeation and retaining a topical effect. We demonstrate this proof of concept via permeation cell tests, histology, Raman microscopy and photoluminescence after application on porcine ear skin.

**Keywords:** topical administration; skin penetration; apatite nanoparticles; permeation; calcium phosphate

## 1. Introduction

Skin is an essential natural barrier of the body. It ensures the isolation of internal organs from the external environment – potentially containing aggressive agents – while allowing major exchanges of water, heat and mineral salts. When the integrity of the skin is compromised due to disorders such as eczema, acne, psoriasis, contact dermatitis, etc., the fundamental roles of this cutaneous barrier are no more ensured, which may lead to health complications including with the development of pathogenic microorganisms. In the field of dermatology, two types of administration routes are customarily used to treat such skin disorders via the delivery of active agents: oral and topical (i.e. via direct application onto the skin). Despite their efficacy to treat the cutaneous tissue, drugs administered by oral administration are however often associated with side effects affecting other cells or organs (e.g. teratogenicity, articular and muscular pain, dryness, altered effectiveness of contraceptive pills, etc. [1, 2]). Therefore, the topical approach is often privileged, at least in a first intention, with the objective to directly apply the active agents onto the affected site of the dermatosis.

However, even for topical administration, the permeation of active ingredients (AI) into the blood circulation may occur in part, thus leading to adverse effects of the drugs as in the systemic route [3]. Transcutaneous drug penetration is dependent on several factors such as the nature of the AI and its state in the pharmaceutical formulation. Most galenic products presently available on the market are based on “simply” solubilized active ingredients which may thus potentially penetrate across the skin and up to the blood circulation.

One appealing approach could be the association of drugs with carrier particles to focus the therapeutic activity on the surface of the skin, thus reducing undesirable effects; and carrier particles can also help to protect unstable AI. In recent years, a considerable interest has grown on the use of particles to target hair follicles for local drug delivery [4], in link with different pathologies such as acne, alopecia, hirsutism and hypertrichosis. Particles properties can be adapted to enhance follicular penetration and one key factor is their size. Wosicka *et al.* [4] reported several studies on particles with different sizes for follicular penetration. Results do not necessarily follow a trend due to the different application techniques used (skin models, application techniques...) and the variety of materials. For example, Vogt *et al.* [5] studied the penetration of fluorescent polymeric microspheres and showed that small particles (< 40 nm) penetrate deeper into the follicle than larger particles ( $\geq 750$  nm). On the other hand, Patzelt *et al.* [6] demonstrated that other types of polymer particles with sizes between 400 and 700 nm penetrate deeper into pig ear skin than smaller particles. Some studies have focused on lipidic

particle such as liposomes. Yang *et al.* [7] studied liposomes to transport free fatty acids such as lauric acid with antimicrobial activity [8]; this vehicle having the advantage of fusing directly with the membrane of the bacterium to deliver AI directly into it for an antibacterial action. Oleosomes were also used, for example by Castro *et al.* [9] as a vector of retinoic acid, and a comedolytic and anti-irritant action was pointed out [10, 11].

Some studies have also been carried out with inorganic particles, which may exhibit greater chemical and/or physical stability than organic-based systems. A new process of selective photothermolysis has recently been published [12], leading to inorganic particles based on silica-gold core-shell with a size closed to 150 nm. Under the action of ultrasound, the nanoparticles, that remained on the surface, penetrated the hair follicle. After laser irradiation, particle temperature increased and caused sebaceous glands destruction. Other organic/inorganic materials have been studied. AI protection, such as retinoic acid, was the subject of a study by Perioli *et al.* [13], by the use of a hydrotalcite-type material consisting of two-dimensional lamellar hydroxides with integrated anti-inflammatory agents [14].

With the view to develop intrinsically-biocompatible inorganic-based particles for skin topical action, the present contribution investigates the use of submicron systems based on bio-inspired calcium phosphate apatites. The bio-inspired character of synthetic nanocrystalline apatites arises from their similarity to the mineral component of bones [15]. Previous works on such apatite colloidal particles have been carried out in the fields of oncology, hematology, medical imaging, gene transfection etc. [16-23], and pointed out their non-cytotoxicity, non-proinflammatory and hemocompatible characters *in vitro*. This aim of this work is to explore the original use of such bio-inspired apatite particles in dermatology, with the specific objective to target a superficial effect avoiding transcutaneous permeation of the drug.

## 2. Materials and Methods

### 2.1. Synthesis of bio-inspired apatite colloids

Colloidal apatite submicron particles were synthesized using phosphonated polyethyleneglycol (PEG)<sub>p</sub> as described in a previous work [19]. Briefly, the apatite precipitation was carried out in deionized water, at room temperature and pH 9.5. After mixing a calcium nitrate solution containing the dispersing agent (PEG)<sub>p</sub> of molecular weight 5200 Dalton, using a molar ratio (PEG)<sub>p</sub> / Ca = 0.0016, into a solution of ammonium dihydrogen phosphate (Ca/P = 0.33), the pH was adjusted to 9.5 by addition of ammonia. The sample was

then placed in a hermetically-closed vial, in an oven at 100°C for maturation of 16 h. After this ageing step, colloidal suspensions were purified by dialysis process to remove unreacted salts [24]. The final pH of each colloid was finally adjusted to physiological pH with a solution of HCl (0.01 M). For comparative assessments, as discussed in the text, a non-colloidal apatite sample was also prepared in this study, by following exactly the same procedure as above, but in the absence of the (PEG)<sub>p</sub> dispersing agent.

## 2.2. Physico-chemical characterization of colloidal particles

The structure of the calcium phosphate particles obtained was determined by powder X-ray diffraction using an INEL Equinox 1000 diffractometer, equipped with a curved counter (2 hours of acquisition), with a cobalt anticathode ( $\lambda_{Co} = 1,78892\text{\AA}$ ). For complementary phase characterization, Fourier transform infrared (FTIR) spectroscopy analyses were performed on a Thermo-Nicolet 5700 spectrometer with a resolution of  $4\text{ cm}^{-1}$ , in the wavenumber range of  $400 - 4000\text{ cm}^{-1}$ , using the KBr pellet method. The chemical composition of the colloidal samples was investigated via atomic absorption spectroscopy (AAS) in flame mode using an Analytik Jena AG – contrAA 300 high-resolution continuum source spectrometer. Initial dissolution of the compounds was performed by acidification with addition of HNO<sub>3</sub> down to pH  $\sim 2$ . Dynamic light scattering was realized with a Nanosizer ZS apparatus (Malvern Instruments,  $\lambda = 630\text{nm}$ ) to determine the hydrodynamic diameter (denoted “particle size” hereafter) of the particles. Transmission Electron Microscopy (TEM) observations were made using a Hitachi HT 7700 microscope. Solid state NMR <sup>31</sup>P was used to further explore the interaction between the surface of apatite particles and the phosphonate endgroup of the (PEG)<sub>p</sub> molecules used here for colloidal stabilization. The NMR spectra were recorded on a Bruker Avance 400 (9.4T) spectrometer (161.76 MHz, MAS mode): the samples were placed in 3.2 mm zirconia rotors rotating at 14 kHz. The experiments were carried out at room temperature. Chemical shifts were determined relatively to 85% H<sub>3</sub>PO<sub>4</sub>.

## 2.3. Cutaneous application: study of permeation and localization of particles

*Skin explants:* *Ex vivo* permeation and localization studies were carried out on porcine ear skin provided freely for the sake of research by two different local slaughterhouses (Bortigali, Sassari, Italy and Puylaurens, France); the use of skin tissue providing from already dead animals is thus in accordance with ethical rules. The ear skin pre-treatment consisted of washing them with cold water and an antibacterial solution (Cytéal®, Pierre Fabre) in order to rinse them and eliminate any impurity. The ears were sheared in a way to not interfere with the penetration

study. The permeation study was carried out on epidermis only. For the permeation study, the ears were soaked in a water bath at 60°C for 2 minutes in order to facilitate the separation of epidermis and dermis. They were dried, and epidermis was separated from dermis by manual gentle pulling [25]. For particle localization assays, biopsies were prepared with a scalpel to withdraw the whole skin (epidermis, dermis and hypodermis). Explants were placed at -20 ° C until use (< 1 month). Each skin sample was then examined under an optical microscope to verify the absence of holes which could alter the permeation studies.

*Permeation study:* Folic acid (FA) was used as a model drug, adsorbed on the surface of the (PEG)<sub>p</sub>-stabilized colloidal particles. The relevance of selecting FA as a model drug here relies in the easiness to titrate it by UV spectroscopy (at  $\lambda = 280$  nm) and to the fact that adsorption of FA onto the surface of (non-colloidal) biomimetic apatites was recently proven to be effective [26]. The colloids were obtained from the reference protocol indicated earlier (part 2.1.), with the only difference of addition of FA in the calcium salt solution (4,87 mmol of  $\text{Ca}(\text{NO}_3)_2 \cdot 4\text{H}_2\text{O}$ , 0.076 mmol of (PEG)<sub>p</sub> and 0.011 mmol of FA in a total volume of 18.75 mL, pH = 9.5), as previously reported using 2-aminoethylphosphate as stabilizing agent [21]. After purification by dialysis, the permeation of these FA-functionalized colloidal apatite particle across synthetic and biological membranes was compared to permeation of a simple FA solution with a concentration of 200 mg/L prepared in a pH = 7.4 buffer medium ( $\text{KH}_2\text{PO}_4 / \text{NaOH}$ , pH ~ 7.4). The amount of FA permeated at each time point was determined by data extrapolation using a calibration curve obtained with FA standard solutions at pH 7.4. The curve was linear in the range of 0.99 –14.85 mg/L ( $y = 0.0631x - 0.0088$ ;  $R^2$  0.99999) and all measurements fell within this range. Sink conditions have been verified for our static and dynamic permeation studies with diffusion cells. Several synthetic membranes were used in this work: two hydrophilic membranes of distinct porosities, 0.05  $\mu\text{m}$  pore size (polycarbonate) and 0.2  $\mu\text{m}$  (cellulose acetate), and one hydrophobic membrane (Strat-M®, Merck Millipore). The latter is constituted of two layers of polyethersulfone (PES) on the surface of a layer of polyolefin, and is pre-impregnated by synthetic lipids, creating a porous structure with a gradient of porosity and susceptible to mimic the partially lipophilic properties of natural skin [27].

Membrane pore size ( $\mu\text{m}$ )	Membrane type	Membrane thickness ( $\mu\text{m}$ )
0.05	Polycarbonate	n.d.
0.2	Polyamide (nylon)	n.d.
0.2	Cellulose acetate	n.d.
n.d.	Polyethersulfone and polyolefin (Strat-M <sup>®</sup> )	300

**Table 1:** List of synthetic membranes tested for the *in vitro* permeation study

Two setups were used in a complementary manner to run the permeation tests, respectively under static and dynamic conditions. For the static permeation overview, a measurement bench of six vertical Franz cells (Microette de Hanson), each consisting in a donor compartment and an accepting compartment (maximum effective volume 6.7 ml) separated by a membrane, was used at the Faculty of Pharmacy of Toulouse. The cells were hermetically closed and thermostated at  $32.0 \pm 0.5^\circ\text{C}$  (typical skin surface temperature). The surface area of diffusion was  $1.76 \text{ cm}^2$  (membrane surface of  $3.14 \text{ cm}^2$  partially covered by the upper O-ring). Each recipient compartment was filled with a buffer solution having a pH close to the physiological value (250 mL of  $\text{KH}_2\text{PO}_4$  0.2M mixed with 195.5 mL of NaOH 0.2M completed with deionized water to reach 1L) and magnetically stirred. For each sampling of the solution, over a time period of 48 h, a similar volume of thermostated buffer was added to maintain the total volume unchanged. For the dynamic permeation study, permeation test cells developed at the Department of Chemistry and Pharmacy of the University of Sassari (Italy) were used [28]. Three permeation cells (vertical-diffusion type) were mounted in parallel and connected to a UV-visible spectrophotometer (Shimadzu UV-160A) as in-line drug monitoring system. As for the static conditions, the whole system is thermostated to  $32.0 \pm 0.5^\circ\text{C}$ . The diffusion area was of  $3.14 \text{ cm}^2$ . Each cell was slightly raised on one side to avoid air bubbles directly beneath the membrane. The donor compartments were partially covered with a plastic stopper in order to avoid evaporation of the samples analyzed. Each recipient compartment was filled with the same buffer solution as above, at a pH close to the physiological value. A magnetic stirrer was placed in the receiver compartment, in addition to the peristaltic pump system to which the cells are connected. The total circulating volume was here of 50 mL with a flowrate fixed at 6 mL/min. The diffusion kinetics of a solution of FA alone (200 mg/L) and of FA adsorbed on the colloidal particles was studied over 2 h (time required for reaching a steady state), with an

initial volume of 1 ml in the donor compartment. Before use, the skin explants were thawed at room temperature and then rehydrated in the medium used in the cell receptor chamber. The explants were then placed on diffusion cells. All experiments were carried out at least in triplicate.

*Localization of particles on skin samples:* Colloidal apatite particles were here doped with europium ions  $\text{Eu}^{3+}$  used so as to follow their localization on skin samples by photoluminescence. Colloids were obtained from the reference protocol indicated earlier (part 2.1.), with the only difference of substitution of a part of calcium ions by europium ions in solution A ( $\text{Ca}(\text{NO}_3)_2 \cdot 4\text{H}_2\text{O} + \text{Eu}(\text{NO}_3)_3 \cdot 5\text{H}_2\text{O} = 4.87 \text{ mmol}$ ) as previously reported for other nanomedicine studies [20, 29]. After purification by dialysis, the localization of the colloidal particles after application onto porcine ear skin explants was investigated from the luminescence signature of  $\text{Eu}^{3+}$ . Comparisons were made with a solution of europium nitrate containing free  $\text{Eu}^{3+}$  ions. Skin samples were used directly after biopsies. The colloidal particles or the europium solution were applied on the skin samples with 1-min manual massage followed by an air drying step at ambient temperature, to simulate the potential use conditions. Skin samples were then cut, placed in resin-containing molds (Tissue-Tek® OCTTM (Optimum Cutting Temperature)) and then frozen by rapid freezing in isopentane cooled to  $-80^\circ\text{C}$  by an ultra-fast freezing system, Snapfrost®. Serial sections of  $5 \mu\text{m}$  thickness were then made using a cryostat (Leica CM 1950), of which half was stained with hematoxylin-eosin (HE) for *histological observation* in order to be able to locate hair follicles and the other half left uncolored for observation by confocal Raman microscopy and photoluminescence. The histological staining of the samples was carried out by the CPTP laboratory, Toulouse, France. The staining was carried out using a coloring automaton (Leica ST 5020) on the cryo-cuts brought back to room temperature (4 minutes in a hematoxylin bath to allow its fixation at the cell nuclei and 2 minutes in a 2% (v/v) eosin solution). After staining, the tissues were dehydrated in two successive  $100^\circ$  ethanol baths, followed by 2 xylene baths, and mounted on slats with Eukitt resin.

The optical analysis of the colored sections was done using an Olympus BX50F microscope. This analysis was carried out in order to identify the hair follicle sections and then to analyze the sections not colored by confocal Raman microscopy. Raman spectra were obtained using a Labram HR800 Horiba Jobin Yvon confocal microspectrometer on samples exposed to a green laser with a wavelength of 532 nm (13 mW, 600 lines/mm). A lens (x100) with a numerical aperture of 0.9 gave a lateral resolution of  $0.7 \mu\text{m}$  and an axial resolution of

2.6  $\mu\text{m}$ . The 3D mappings were made with a 532 nm 13 mW laser, a 3  $\mu\text{m}$  pitch and an acquisition time of 3 s and 1 accumulation. All spectra were processed using the LabSpec6 software.

#### 2.4. Statistics

Permeation tests were carried out on a minimum of triplicate assays. The reproducibility of batch synthesis was assessed by running some permeation experiments on two different batches of colloidal apatite particles, each in triplicate. Permeation data are plotted in mean  $\pm$  standard deviation.

### 3. Results and discussion

#### 3.1. Colloidal particles characterization

We have previously reported particle size data on colloids stabilized by (PEG)<sub>p</sub>, around 200 nm for (PEG)<sub>p</sub> 5200 g/mol before purification by dialysis [19]. Additional characterization of the colloidal particles was performed here after dialysis. First of all, atomic absorption spectroscopy coupled with gravimetric results (measurement of the dry powder mass obtained after complete lyophilization of a colloid of 25 mL) allowed us to determine the molar ratio between (PEG)<sub>p</sub> and the apatite phase in these colloids, which is of the order of (PEG)<sub>p</sub> / apatite = 0.12.

The XRD pattern of the particles stabilized with (PEG)<sub>p</sub> was recorded after dialysis purification and freeze-drying (**Figure 1**). Comparison with a reference pattern for a non-colloidal sample, prepared under same conditions but in the absence of the (PEG)<sub>p</sub> dispersing agent, indicates in both cases the presence of a moderately-well crystallized apatitic phase (highly similar to that of bone mineral [15, 30]). A slight decrease of crystallinity can be observed for colloidal particles compared to the reference (especially on peaks (211), (112) and (300)). This decrease associated with the presence of (PEG)<sub>p</sub> during apatite precipitation can be evaluated by applying the ISO 13779-3: 2008 standard (compared to sintered stoichiometric hydroxyapatite), leading to a degree of crystallinity of  $82 \pm 4$  % for the colloidal particles and  $89 \pm 5$  % for non-colloidal apatite (reference). It points out the existence of an interaction between the (PEG)<sub>p</sub> molecules and the apatite crystals in formation during the precipitation stage. The XRD pattern of the colloid (lyophilized) also shows peaks of the dispersing agent

(PEG)p as indicated by the comparison with the diagram obtained on the pure (PEG)p reagent (**Figure 1**). Application of Scherrer's equation [31] to peaks (002) and (310) demonstrates the nanometric dimensions of the crystallites composing the colloidal sample, with an average length along the c axis of the apatite around  $24 \pm 2$  nm and a mean width/thickness around  $12 \pm 2$  nm. These results thus reveal crystallites of nanometric sizes as in bone mineral (biomimetic character [15]) for these colloidal particles.

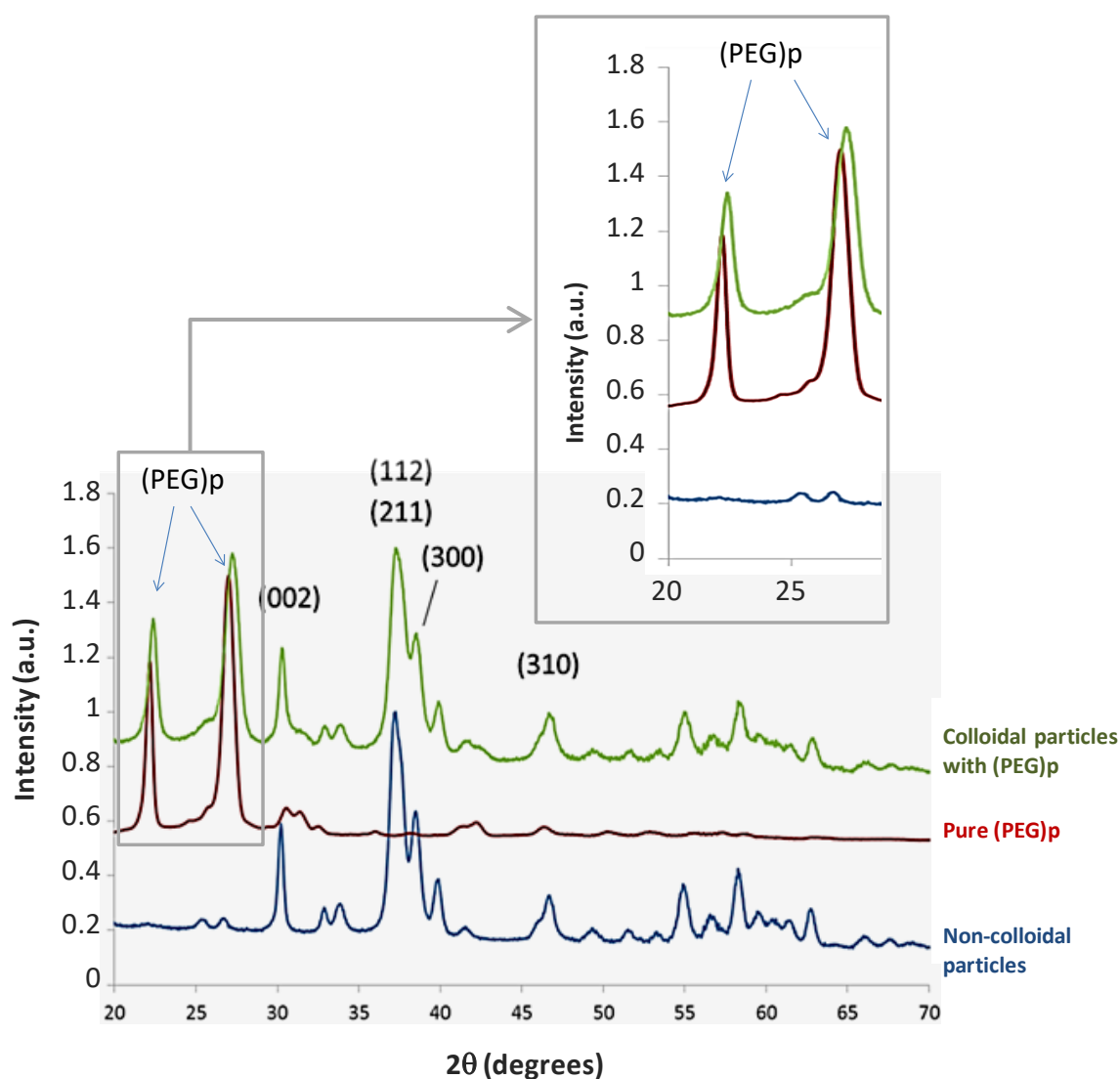


**Figure 1:** XRD patterns for colloidal and non-colloidal apatite particles and for pure (PEG)p (MW 5200 g/mol). The inset shows a zoom on the  $2\theta = 20\text{-}28^\circ$  range unveiling specific diffraction peaks of (PEG)p

Complementary assessments were obtained via FTIR spectroscopy. As shown in **Figure 2**, characteristic apatitic vibration modes  $\nu_3(\text{PO}_4)$  and  $\nu_4(\text{PO}_4)$  can easily be identified for the colloidal particles, by comparison to the spectrum obtained on non-colloidal apatite. Moreover,

the characteristic bands of (PEG)p are also found on the FTIR spectrum of colloidal particles as witnessed by reference to pure (PEG)p. Nevertheless changes in spectral features of colloidal and non-colloidal apatite can be seen: the spectral signature of apatitic hydroxide ions visible at  $3572\text{ cm}^{-1}$  ( $\nu_s(\text{OH}_{\text{ap}})$ ) and  $632\text{ cm}^{-1}$  ( $\nu_l(\text{OH}_{\text{ap}})$ ) is in particular less intense for the colloid (e.g. see zoom in **Figure 2**), which could be related to a lower content of  $\text{OH}^-$  apatitic ions, suggesting in turn a lower degree of stoichiometry of the apatite phase. This is probably linked to the lower crystallinity evidenced by XRD in **Figure 1**, and these data suggest some crystal growth inhibition played by the (PEG)p organic moiety. A decomposition of the FTIR spectrum between  $500$  and  $700\text{ cm}^{-1}$  of the colloidal particles was carried out using a methodology previously developed for the study of biomimetic nanocrystalline apatites [32] (**Figure 3**). Several contributions associated to the vibration of  $\text{PO}_4^{3-}$  ions (apatitic typically at  $560$ ,  $575$  and  $601\text{ cm}^{-1}$ , and not apatitic at  $617\text{ cm}^{-1}$ ),  $\text{HPO}_4^{2-}$  (apatitic at  $550\text{ cm}^{-1}$  and not apatitic at  $534\text{ cm}^{-1}$ ), and  $\text{OH}^-$  ( $632\text{ cm}^{-1}$ ) are seen in this domain. From this decomposition, the area of each contribution was evaluated by spectral decomposition using the ORIGIN® 8.5 software. It is then possible to determine the relative proportion occupied by ions in a given sample. The ratio  $R$  of the integrated intensities for the  $\text{OH}^-$  apatitic ions can be defined by:

$$R = \frac{\text{OH}^- \text{ap}}{\text{OH}^- \text{ap} + \text{PO}_4^{3-} \text{ap} + \text{HPO}_4^{2-} \text{ap}} \quad \text{Equation 1}$$

Equation 1 gives the relative proportion of  $\text{OH}^-$  apatitic ions contained in the samples, leading to a value of 0.39 for the non-colloidal reference apatite and 0.29 (after subtraction of the contribution of (PEG)p) for colloidal apatite. These values confirm a significant decrease in the proportion of  $\text{OH}^-$  ions in the apatitic phase obtained by the colloidal route compared to the non-colloidal compound. Moreover, the samples prepared here at  $100^\circ\text{C}$ , during 16h (either in the absence or in the presence of (PEG)p) do not exhibit a significant spectral contribution for  $\text{HPO}_4^{2-}$  ions, as evidenced by the very low peak area centered on  $534$  and  $550\text{ cm}^{-1}$ , suggesting that in this work the apatite crystals do not exhibit an extended hydrated ionic layer on their surface.

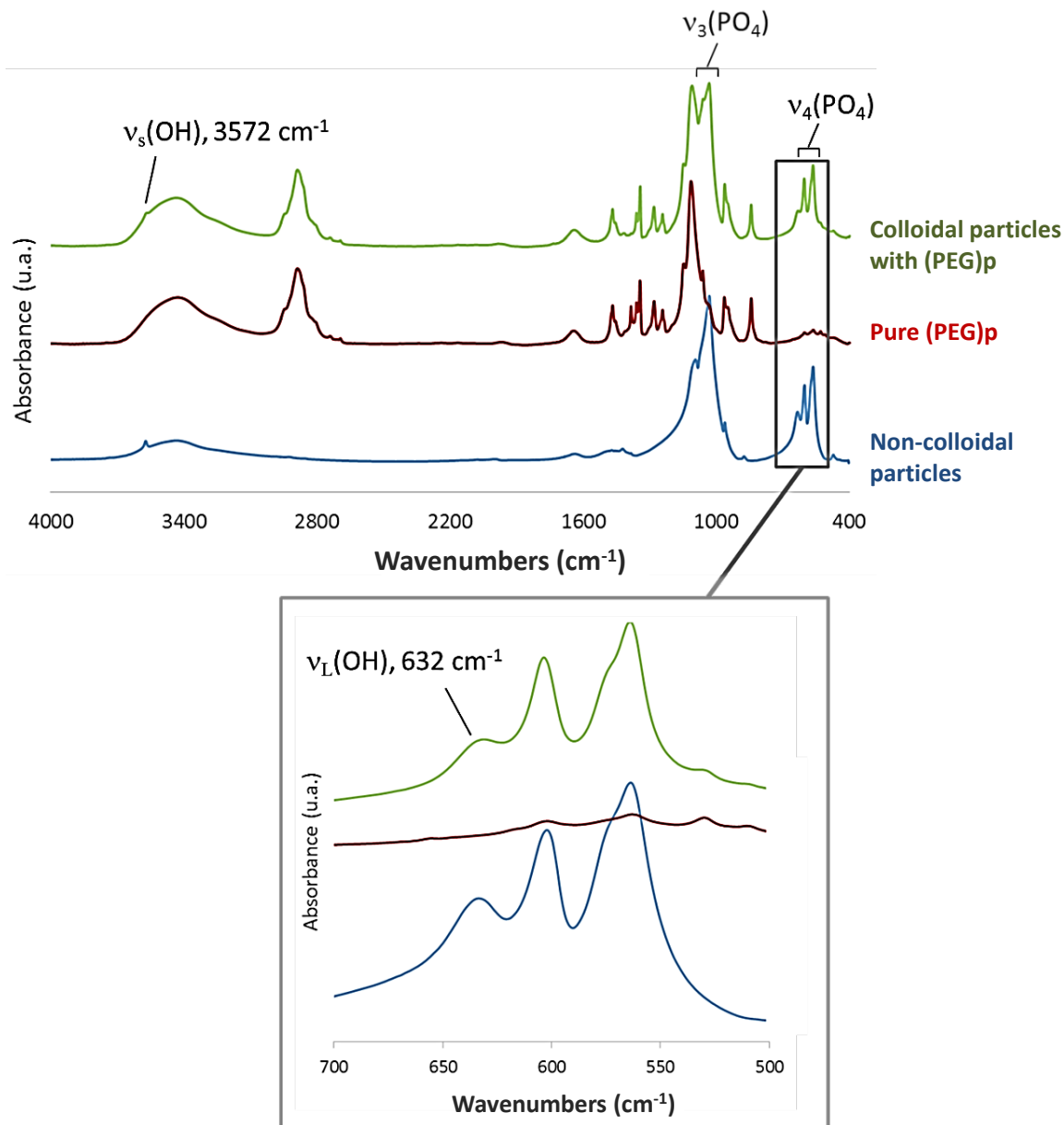


**Figure 2:** FTIR spectra for colloidal and non-colloidal apatite particles and for pure (PEG)p (MW 5200 g/mol). The inset shows an enlargement of the 500-700  $\text{cm}^{-1}$  range

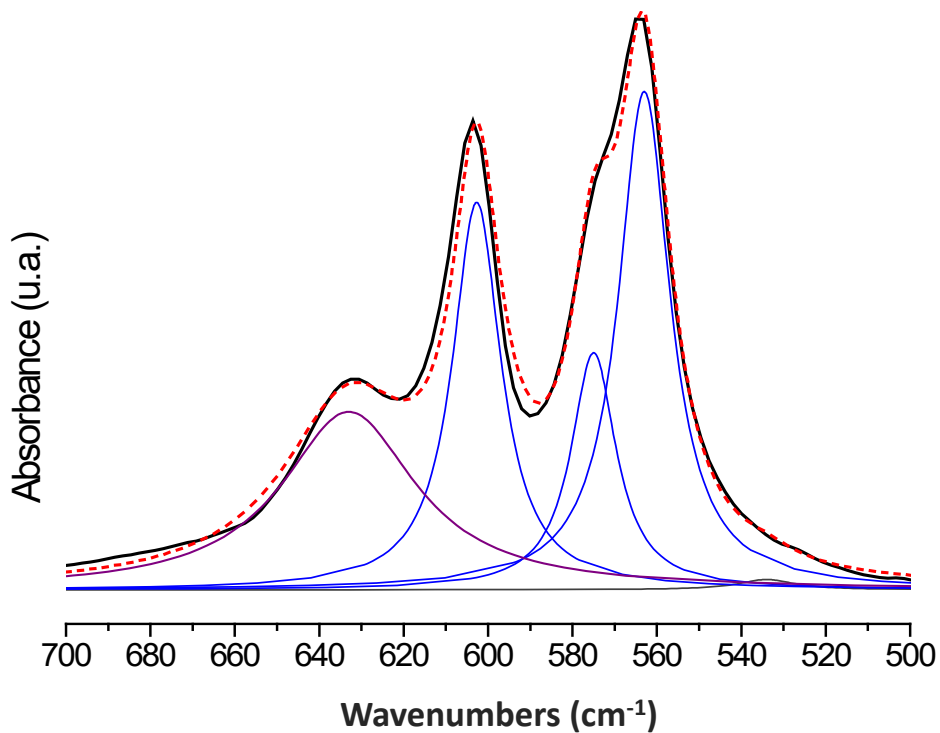


**Figure 3:** Spectral deconvolution of colloidal apatite particles stabilized by (PEG)<sub>p</sub>, in the  $\nu_4(\text{PO}_4)$  spectral domain ( $500\text{-}700\text{ cm}^{-1}$ )

Solid state  $^{31}\text{P}$  MAS-NMR spectroscopy was used to investigate further the interaction between the phosphonated termination of the (PEG)<sub>p</sub> molecules and the surface of apatite particles. **Figure 4** shows the spectra obtained for a colloid stabilized with (PEG)<sub>p</sub> 5200 and for (PEG)<sub>p</sub> alone. The spectrum relating to (PEG)<sub>p</sub> alone shows the presence of two main peaks at 30.6 and 3.9 ppm. The colloidal particles have in contrast an intense peak localized at 2.7 ppm and a large peak of lower intensity with a maximum at 24.2 ppm. The peak at 2.7 ppm is attributed to apatitic phosphates [33]. The second peak (at 24.2 ppm) cannot be imputed to the phosphate ions of apatite and has to be associated to the presence of (PEG)<sub>p</sub>, indicating a modification of the spectral signature of this molecule when interacting with the surface of apatite particles. The initial (PEG)<sub>p</sub> peak at 30.6 ppm thus appears to be enlarged and shifted to lower chemical shifts, unveiling the existence of a strong interaction between the phosphonate group of (PEG) and the apatite crystal surface, therefore favoring an orientation of the molecule with the phosphonate end-group toward the surface of the particles and the organic PEG chain hanging toward the solution.

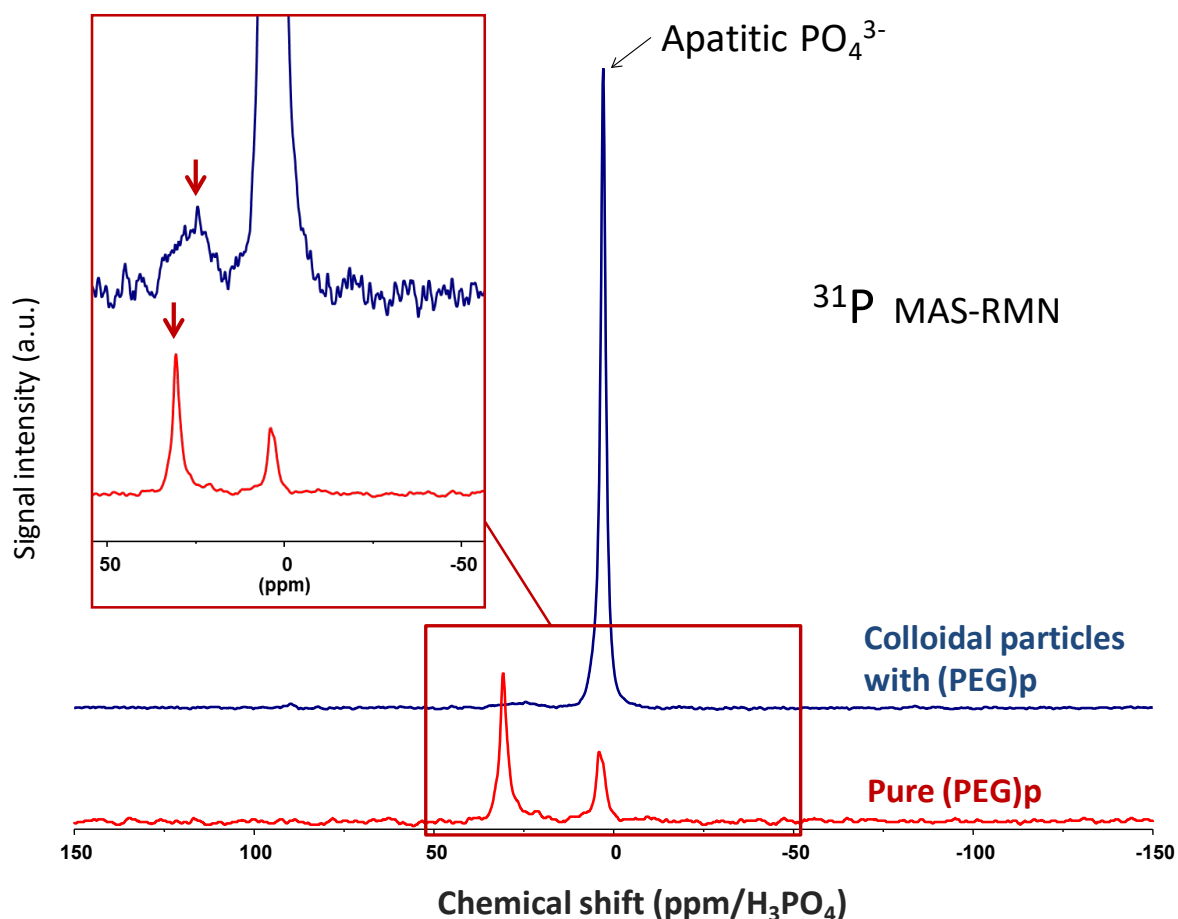


**Figure 4:** NMR  $^{31}\text{P}$  spectra for colloidal apatite stabilized with (PEG)p and for pure (PEG)p (MW 5200 g/mol)

The mean hydrodynamic diameter of the colloidal particles was measured before dialysis, reaching 240 nm with a polydispersity index of 0.22. Measurement performed after dialysis showed a downshift to about 180 nm with a lower polydispersity index of 0.17. The mean diameter and the polydispersity of the sample were thus slightly decreased, potentially due to a reorganization of the organic corona around the particles (indeed, a partial dissolution of the particles would have instead been associated to an increase in particle size due to the partial release of some stabilizing (PEG)p molecules which is not seen here). TEM was tentatively used for a more direct observation of the particles; however it was difficult to find sample preparation conditions (deposition and drying on the copper grid) and analysis conditions (time under high vacuum) that did not alter the particles by provoking their partial desegregation into smaller pieces (**Figure S1**).

### 3.2. Permeation study across synthetic and biological membranes

A permeation study was then undergone to check the crossing of a model drug, Folic Acid (FA) adsorbed on the colloidal particles, across synthetic and biological membranes using diffusion cells. In a first step, Franz cells were used, under static conditions. The stability of the FA solution in the used buffer solution was preliminarily verified by confirming the steadiness of the absorbance over 48 h. Several synthetic membranes were tested here so as to evaluate the impact of membrane characteristics, such as their hydrophilicity and porosity, on the permeation of the particles (**Table 1**). The use of artificial model membranes indeed offers a simple and reproducible alternative to study the basic physicochemical mechanisms of drug permeation without the intra- and inter-individual variations related to the use of isolated skin portions from human or animal origin, as stated by Flaten *et al.* [34].

The kinetic permeation study (titrating FA in the recipient compartment by UV-vis spectrophotometry) was first carried out on an FA solution, i.e. in the absence of particles. The data pointed out the clear impact of the hydrophilic/lipophilic nature of the test membranes (**Figure 5a**): while similar kinetics were found for the two hydrophilic membranes (~90% permeation at 24 h), diffusion through the Strat-M® membrane remained very low (< 5% at the same timepoint). Although they have shown a certain capacity to mimic cutaneous permeation [35], results may differ from data obtained on actual human skin depending on experimental conditions. In order to allow a more discriminative comparison of the permeation data obtained in this work using FA as model drug, hydrophilic synthetic membranes were judged more relevant for the rest of this study.

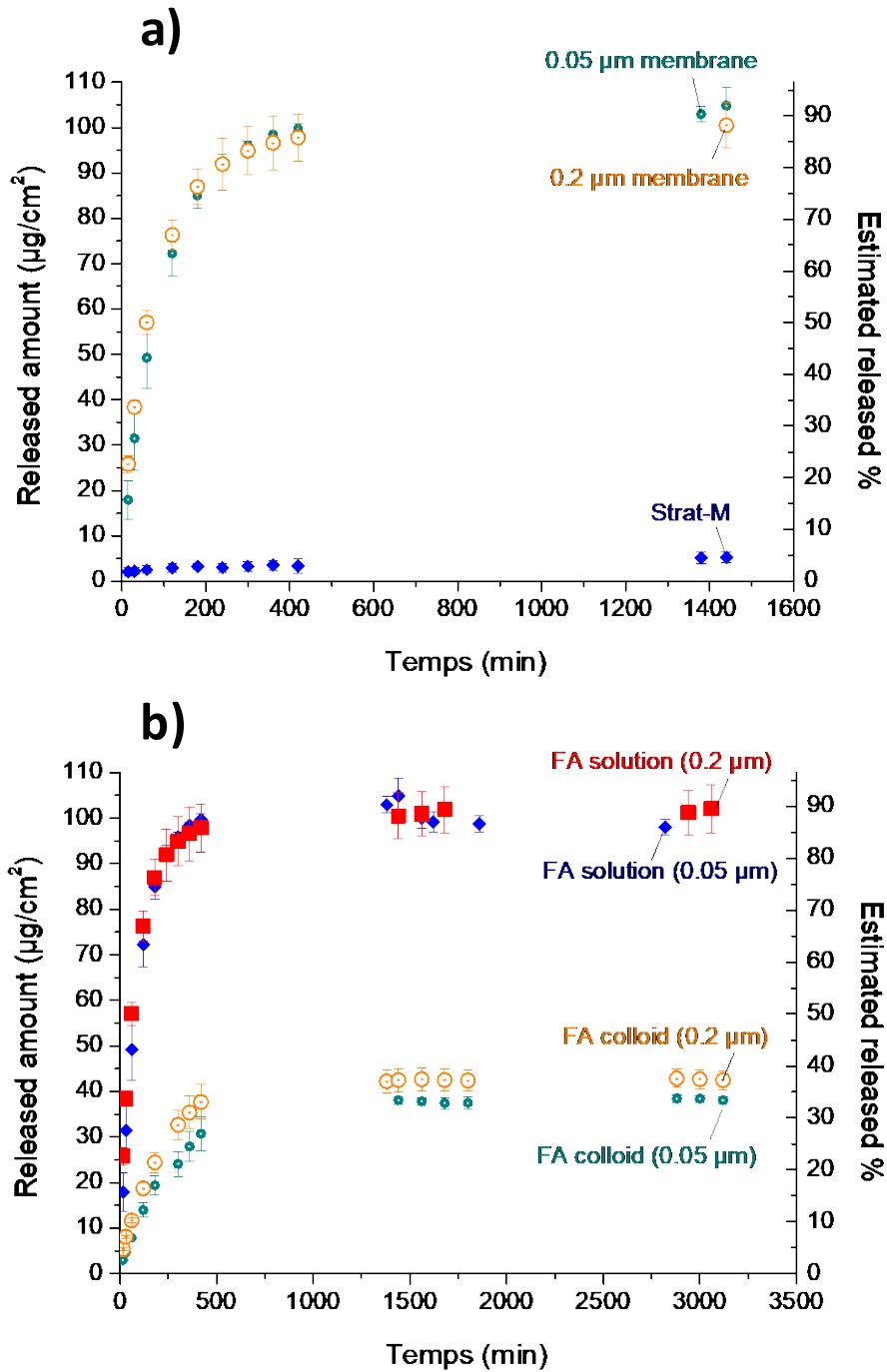


**Figure 5:** a) Permeation of an FA solution (200 mg/L of FA prepared in phosphate buffer  $\text{KH}_2\text{PO}_4 / \text{NaOH}$ , pH  $\sim 7.4$ ) across 3 synthetic membranes, in static conditions. b) Permeation of FA solution and FA-functionalized colloidal particles across the two synthetic hydrophilic membranes (0.05 and 0.2  $\mu\text{m}$  porosities), in static conditions.

**Figure 5b** reports the permeation data for the two hydrophilic membranes with both FA solution and the FA-loaded colloidal apatite particles (FA loaded dose: 25  $\mu\text{mol/g}$ ). The presence of this small amount of FA is not detectable by XRD nor FTIR analyses. DLS analyses after dialysis showed a mean hydrodynamic diameter of 193 nm. Interestingly, as shown in **Figure 5b**, the diffusion rate was found to be significantly reduced for FA adsorbed on the colloidal particles (plateau reached at  $\sim 1500$  min) compared to the a solution of free FA molecules (stabilization around 400 min). Also, the released FA amount reached only an estimate of 34 to 38% for the colloid as opposed to 90% for the solution. It may be noted that these conclusions are valid for both membrane porosities tested. These findings thus support the strategy developed in the present paper, aiming to limit the drug permeation via the preliminary adsorption onto apatite submicron particles.

To better quantify the permeation data across the two membranes, the corresponding effective permeation coefficients  $P_{eff}$  were calculated ( $\text{mg}\cdot\text{cm}^{-2}\cdot\text{min}^{-1}$ ) via the equation [36]:

$$P_{eff} = \Delta \cdot \frac{V}{A \cdot C_D}$$

where  $\Delta = (dC/dt)_{ss}$  is the variation of the concentration as a function of time at stationary state ( $\mu\text{mol}\cdot\text{mL}^{-1}\cdot\text{min}^{-1}$ ),  $V$  is the volume of the recipient compartment (mL),  $A$  is the diffusion area ( $\text{cm}^2$ ) and  $C_D$  the initial concentration in the donor compartment ( $\mu\text{mol/mg}$ ). The values of  $P_{eff}$  calculated for the diffusion of the colloidal particles across the membranes with 0.2  $\mu\text{m}$  and 0.05  $\mu\text{m}$  porosities were, respectively, of  $0.63\cdot 10^{-3} \pm 0.07\cdot 10^{-3} \text{ mg}\cdot\text{cm}^{-2}\cdot\text{min}^{-1}$  and  $0.52\cdot 10^{-3} \pm 0.09\cdot 10^{-3} \text{ mg}\cdot\text{cm}^{-2}\cdot\text{min}^{-1}$ . Despite large uncertainties on these values, a lower diffusion rate appears to be reached when decreasing the mean porosity of the membrane, albeit the diffusion across the 0.05  $\mu\text{m}$  membrane remains noticeable. Although DLS gave an averaged mean size around 193 nm (supposing a spherical shape), it may be noted that the particles are not expected to be purely spherical as we previously observed ellipsoidal shapes for colloidal apatite particles obtained by a similar protocol with AEP stabilizing agent (CIRIMAT laboratory, Toulouse, internal communication), thus exposing both a large and a small diameter. Therefore, direct comparison of DLS particle mean size and membrane porosity is not relevant (and TEM analyses led to particle alterations due to the high beam energy, making direct observations rather complex to achieve without affecting the particles). Nevertheless, these  $P_{eff}$  calculations allowed us to quantify the effective permeation rates reached in the static Franz cells conditions.

One possible artifact could however be the desorption of a portion of the FA adsorbed amount during the long diffusion time necessary for this static study. In order to minimize or eliminate this artifact, we accelerated the diffusion study by using permeation test cells in dynamic conditions as described in the experimental section. Using the same two membranes as for the static study, the permeation of a solution of FA was shown to cross the membranes after 10 min for membrane porosity 0.2  $\mu\text{m}$  and less than 30 min for the 0.05  $\mu\text{m}$  membrane, thus considerably faster than above ( $\ll$  400 min) (**Figure S2**). The reproducibility of the study was also cross-checked by running experiments on two different batches of colloidal apatite particles, each in triplicate, showing highly reproducible data (**Figure S3**). For the 0.2 and 0.05  $\mu\text{m}$  membrane porosities, the calculated effective permeation coefficients were respectively of  $89.00 \pm 3.67$  and  $3.27 \pm 0.12$   $\text{mg}\cdot\text{cm}^{-2}\cdot\text{min}^{-1}$  (the plateau being reached in about 1 h in such dynamic conditions). These data thus validated our objective to obtain much faster diffusion rates compared to the static mode, and also pointed to the higher impact of membrane porosity on permeation. The dynamic setup was thus selected for the rest of the study.

In order to progress one more step toward the actual situation of skin permeation, similar dynamic experiments were then carried out on the epidermis layer withdrawn manually from porcine ear skin explants. The sampling of the epidermis (external part of the skin only) was cross-checked by histology coloration (**Figure 6a**), evidencing the absence of dermal sublayers. The permeation of FA was then studied as above, but on these *ex vivo* epidermis samples (**Figure 6b**). Again, fast diffusion was evidenced for FA solution (total amount diffused in  $\sim$ 20 min). In contrast, and most interestingly, when the FA molecules were adsorbed on the colloidal apatite particles, a drastically slower diffusion was detected across this epidermis layer. As for the synthetic membranes, these findings thus demonstrate that having the drug pre-adsorbed onto colloidal apatite particles (as compared to the free solubilized drug) allows limiting radically its epidermis permeation. In our experimental conditions, only *ca.* 10% of FA associated to the particles may cross the epidermis barrier after 2 h of contact.

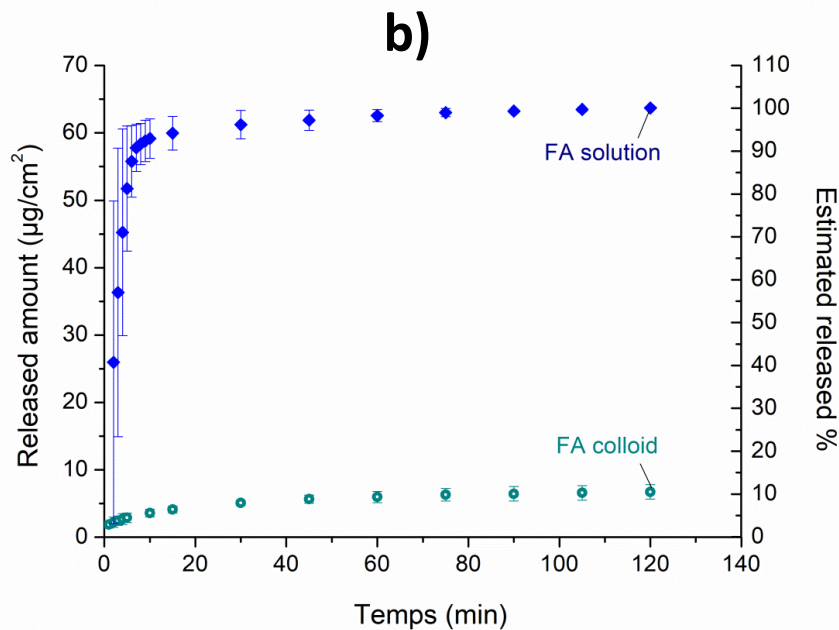
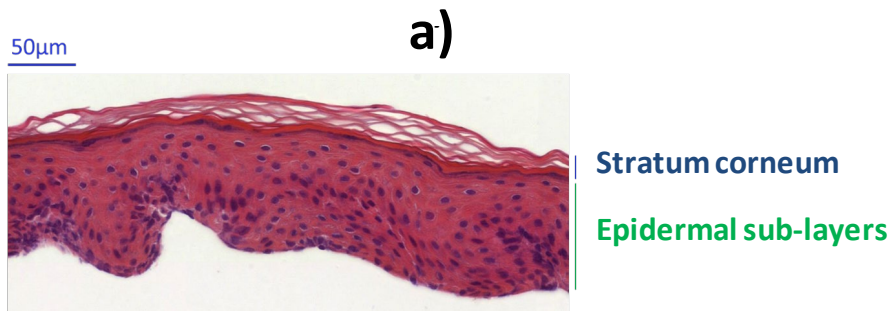


**Figure 6:** a) Epidermis portion of porcine ear skin. b) corresponding *ex vivo* permeation study for FA solution and FA-functionalized colloidal particles, in dynamic conditions

### 3.3. Localization of particles after skin application

Whether using the static or the dynamic setups, all our permeation data evidenced a drastic decrease of the permeation of the drug (here modeled by FA) across synthetic and biological membranes when the drug was associated to the apatite colloidal particles rather than simply solubilized in the medium. In other words, the adsorption of the drug onto the particles surface could allow, in dermatological applications, to retain the drug on the skin surface for favoring a topical effect.

To further demonstrate this point, the localization of apatite colloidal particles after application onto (unfrozen) porcine ear skin explants was followed by histological observations coupled to Raman confocal microscopy. To facilitate this analysis, luminescent  $\text{Eu}^{3+}$  ions were used as

“model drug” and the related photoluminescence linked to the  $^5D_0 \rightarrow ^7F_2$  transition of  $\text{Eu}^{3+}$  was followed. Note that only a few mole percents of  $\text{Ca}^{2+}$  ions ( $\sim 1.5\%$ ) from the apatite particles were substituted by  $\text{Eu}^{3+}$  ions, therefore not modifying the other physical-chemical properties of the particles as shown previously [29]. Preliminary tests showed that the Raman spectrum of porcine ear skin did not lead to bands in the  $605\text{-}627\text{ cm}^{-1}$  domain where  $\text{Eu}^{3+}$  is active. Similar experiments were also carried out using a solution of europium nitrate to mimic the situation of a solubilized drug. **Figure 7** reports the results obtained in these two scenarios:  $\text{Eu}^{3+}$  simply solubilized and  $\text{Eu}^{3+}$  associated to the particles. When europium ions were in the dissolved state in aqueous solution (**Figure 7a**), a dissemination of these ions was noticed not only on the skin surface but also in the infundibulum, the epidermis invagination and in the dermal zone, as witnessed by the blue staining (artificial color) indicating the position of Eu-rich domains. Several Eu-rich large islands (red arrows in **Figure 7a** and **Figures S4**) were observed in this case, traducing significant skin penetration. The Raman spectral signatures obtained by analyzing the blue-colored zones indeed showed the typical luminescence features of  $\text{Eu}^{3+}$  ions (**Figure S5**). In contrast, observations made when the europium was associated to the particles led to a localization of the particles noticeably more pronounced on the skin outer layer and at the entrance of hair follicles (**Figure 7b** and **Figure S6**). No large island rich in europium was observed in this case. These data are thus in good agreement with our permeation studies reported above in static and dynamic conditions on several synthetic membranes and epidermis, pointing to a preferential surface localization of a drug if associated to the particles.

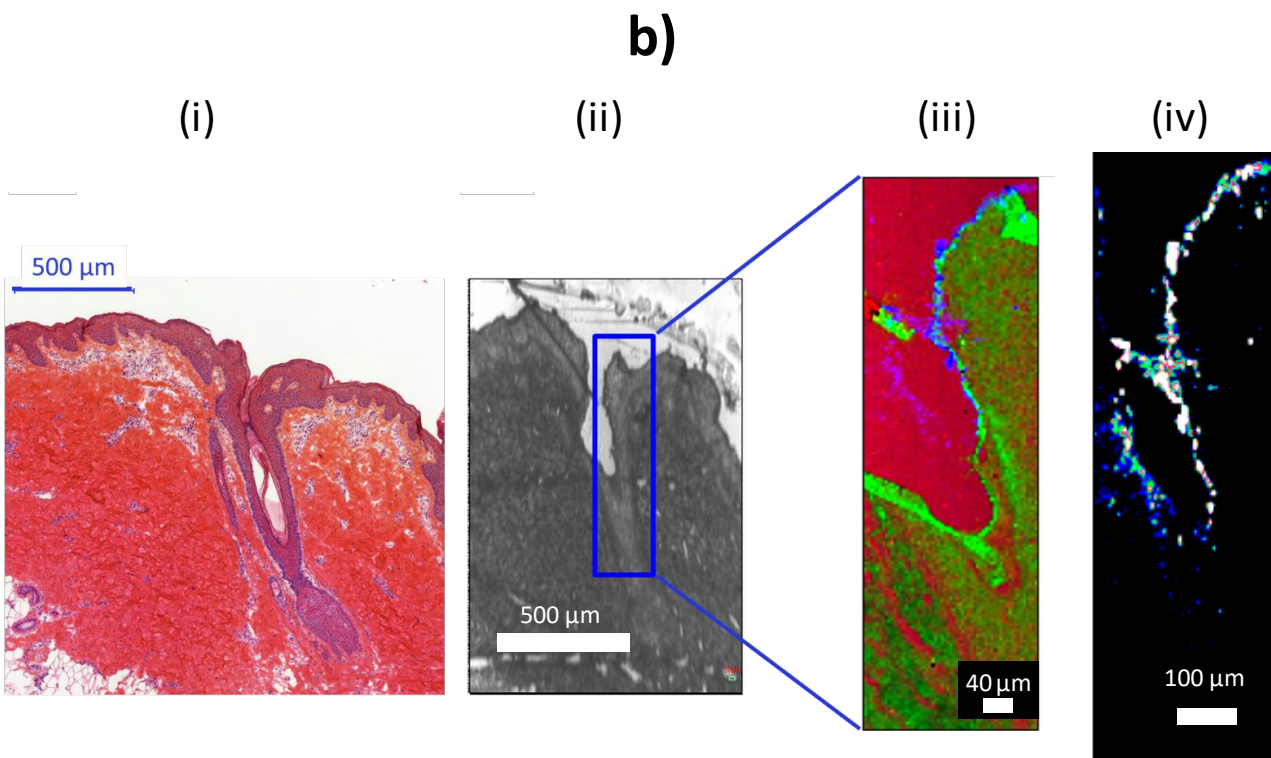
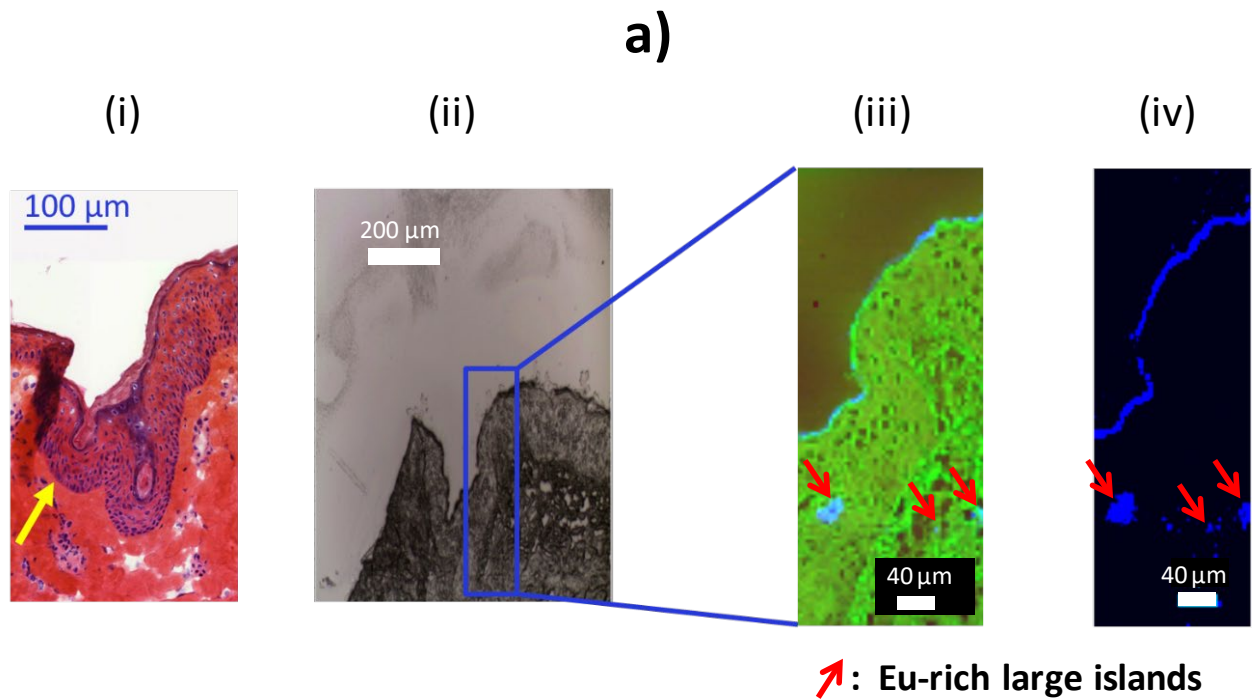


**Figure 7:** Coupled histological/Raman/photoluminescence observations of porcine ear skin explants: a) after application of a  $\text{Eu}^{3+}$  solution. b) after application of Eu-doped colloidal particles. Images (i) were obtained via histological staining (see experimental section). Images (ii) show the corresponding area by optical microscopy. Images (iii) show the distributions of chemical species obtained by Raman spectroscopy where the blue coloration (artificial color)

shows the location of  $\text{Eu}^{3+}$ . Images (iv) show more precisely the localization of the luminescent  $\text{Eu}^{3+}$  ions.

### *3.4. Discussion*

Orally administered drugs access the blood stream and may be associated to various side effects. Topical application is thus a relevant therapeutic strategy in dermatology to limit adverse effects and deliver directly the active components to the skin [37, 38]. However, drug permeation may still occur partially, especially if the therapeutic treatment needs to be applied over an extended period of time [39]. Also, in the context of a dermatitis like acne, the relevance of a topical approach is all the more effective that the pathology is associated with the local development of bacteria at hair follicles [40]. It thus appears sensible to develop strategies to restrain the action of the drug (and thus its localization) on the skin surface. The possibility to deliver the drug directly at hair follicles has been explored with various systems involving drug nanocarriers [4], yet the ideal system still needs to be found. In this work, we have proposed the use of bio-inspired calcium phosphates as drug carrier for topical applications. The particles are composed of nanocrystalline apatite with strong similarity to bone mineral [41] and stabilized by phosphonated polyethyleneglycol (PEG)<sub>p</sub>. These components are highly biocompatible, and the exceptional reactivity of apatite nanoparticles opens the way to a wealth of applications, well beyond bone repair [42].

In a first part of this work, permeation tests carried out in static and dynamic conditions studies using artificial and biological (porcine epidermis) membranes were run. Our data indicate in both cases that association of the drug (here modeled by folic acid, FA) to the apatite nanoparticles drastically reduces the permeated amount as compared to an FA solution with “free” solubilized molecules.

In a second part of the work, we used europium-substituted apatite NPs (europium being used here as a luminescent model “drug”) to investigate the localization of the particles after application on porcine ear skin explants. The use of skin explants for dermatological purposes has been widely developed and used in the literature (e.g. [43]). In our work, in order to follow the particles localization, we developed a strategy coupling histology, Raman confocal microscopy and photoluminescence. Our observations supported the data obtained via permeation tests, suggesting that association of a drug on the NPs surface significantly reduces

skin penetration, thus favoring a skin surface local effect. Indeed, while Eu-rich large islands (red arrows on **Figure 7a**) were observed when applying a europium solution onto the skin explants, unveiling significant skin penetration, the Eu-loaded particles were essentially localized on the skin outer layer and at the entrance of hair follicles (**Figure 7b**). The strategy developed in this work, using colloidal apatite nanoparticles to deliver drugs to the skin for a local delivery while limiting skin penetration, is thus found successful.

#### **4. Conclusions**

Skin disorders may lead to alterations of the cutaneous barrier, and dermatological formulations can be used topically for a local treatment. In order to limit transcutaneous permeation of the drug and related side effects, its association to biocompatible carrier particles appears particularly adapted. In this work, bio-inspired apatite particles (close to the composition of natural bone mineral) exhibiting a high intrinsic biocompatibility were considered for the first time as possible drug carriers for favoring topical skin administration in view of dermatological applications to treat such dermatoses. Using both folic acid and europium as “model drugs”, our data (in terms of drug permeation across synthetic and biological membranes as well as particle localization after skin administration) converge to show that association of the drug to apatite particles may significantly favor skin surface effects. These findings open the way to novel applications of bio-inspired calcium phosphate apatites in the field of dermatology, and participate to show the relevance of mineral-based particles as drug carriers for local delivery to the skin.

#### **Acknowledgement**

M. Choimet thanks the *CIRIMAT* Carnot Institute (now part of the *Chimie Balard CIRIMAT* Carnot Institute) for PhD funding and *Toulouse INP* for the travel grant to Sardinia, Italy. The authors wish to thank the local slaughterhouses in Bortigali, Sassari, Italy and Puylaurens, France for providing porcine ears freely for the sake of research. We thank Dr. Talal Al Saati and Dr. Florence Capilla from the Centre de Physiopathologie de Toulouse-Purpan (CPTP), Toulouse, France, for their support on the histology work. We thank Yannick Coppel, from LCC Toulouse, for support on the NMR analyses.

**Conflict of interest**

The authors declare no competing interests.

**Author declaration**

This submission complies with the Author Declaration.

**Data availability**

The raw/processed data required to reproduce these findings cannot be shared at this time as the data also forms part of an ongoing study.

## References

- [1] R. Nguyen, J. Su, Treatment of acne vulgaris, *Paediatrics and Child Health* 21(3) (2011) 119-125.
- [2] U. Jappe, Pathological mechanisms of acne with special emphasis on *Propionibacterium acnes* and related therapy, *Acta dermato-venereologica* 83(4) (2003) 241-248.
- [3] A. Akhavan, S. Bershad, Topical acne drugs: review of clinical properties, systemic exposure, and safety, *Am J Clin Dermatol* 4(7) (2003) 473-92.
- [4] H. Wosicka, K. Cal, Targeting to the hair follicles: current status and potential, *J Dermatol Sci* 57(2) (2010) 83-9.
- [5] A. Vogt, B. Combadiere, S. Hadam, K.M. Stieler, J. Lademann, H. Schaefer, B. Autran, W. Sterry, U. Blume-Peytavi, 40 nm, but not 750 or 1,500 nm, nanoparticles enter epidermal CD1a+ cells after transcutaneous application on human skin, *J Invest Dermatol* 126(6) (2006) 1316-22.
- [6] A. Patzelt, H. Richter, F. Knorr, U. Schafer, C.M. Lehr, L. Dahne, W. Sterry, J. Lademann, Selective follicular targeting by modification of the particle sizes, *J Control Release* 150(1) (2011) 45-8.
- [7] D. Yang, D. Pornpattananangkul, T. Nakatsuji, M. Chan, D. Carson, C.M. Huang, L. Zhang, The antimicrobial activity of liposomal lauric acids against *Propionibacterium acnes*, *Biomaterials* 30(30) (2009) 6035-40.
- [8] T. Nakatsuji, M.C. Kao, J.Y. Fang, C.C. Zouboulis, L. Zhang, R.L. Gallo, C.M. Huang, Antimicrobial property of lauric acid against *Propionibacterium acnes*: its therapeutic potential for inflammatory acne vulgaris, *J Invest Dermatol* 129(10) (2009) 2480-8.
- [9] G.A. Castro, R.L. Orefice, J.M. Vilela, M.S. Andrade, L.A. Ferreira, Development of a new solid lipid nanoparticle formulation containing retinoic acid for topical treatment of acne, *J Microencapsul* 24(5) (2007) 395-407.
- [10] G.A. Castro, A.L. Coelho, C.A. Oliveira, G.A. Mahecha, R.L. Orefice, L.A. Ferreira, Formation of ion pairing as an alternative to improve encapsulation and stability and to reduce skin irritation of retinoic acid loaded in solid lipid nanoparticles, *Int J Pharm* 381(1) (2009) 77-83.
- [11] G.A. Castro, C.A. Oliveira, G.A. Mahecha, L.A. Ferreira, Comedolytic effect and reduced skin irritation of a new formulation of all-trans retinoic acid-loaded solid lipid nanoparticles for topical treatment of acne, *Arch Dermatol Res* 303(7) (2011) 513-20.
- [12] D. Paithankar, B.H. Hwang, G. Munavalli, A. Kauvar, J. Lloyd, R. Blomgren, L. Faupel, T. Meyer, S. Mitragotri, Ultrasonic delivery of silica-gold nanoshells for photothermolysis of sebaceous glands in humans: Nanotechnology from the bench to clinic, *J Control Release* 206 (2015) 30-6.
- [13] L. Perioli, C. Pagano, M. Nocchetti, L. Latterini, Development of Smart Semisolid Formulations to Enhance Retinoic Acid Topical Application, *J Pharm Sci* 104(11) (2015) 3904-3912.
- [14] V. Ambrogi, G. Fardella, G. Grandolini, L. Perioli, Intercalation compounds of hydrotalcite-like anionic clays with antiinflammatory agents--I. Intercalation and in vitro release of ibuprofen, *Int J Pharm* 220(1-2) (2001) 23-32.
- [15] J. Gomez-Morales, M. Lafisco, J.M. Delgado-Lopez, S. Sarda, C. Drouet, Progress on the preparation of nanocrystalline apatites and surface characterization: Overview of fundamental and applied aspects, *Progress in Crystal Growth and Characterization of Materials* 59(1) (2013) 1-46.
- [16] M. Stefanic, K. Ward, H. Tawfik, R. Seemann, V. Baulin, Y. Guo, J.B. Fleury, C. Drouet, Apatite nanoparticles strongly improve red blood cell cryopreservation by mediating trehalose delivery via enhanced membrane permeation, *Biomaterials* 140 (2017) 138-149.
- [17] C. Drouet, C. Rey, C.I. Combes, S. Cazalbou, S.p. Sarda, D. Grossin, Nanocrystalline apatites: a versatile functionalizable platform for biomedical applications for bone engineering... and beyond, *Key Engineering Materials* 696 (2016) 14-22.
- [18] M.I. Choimet, K. Hyung-Mi, O. Jae-Min, A. Tourrette, C. Drouet, Nanomedicine: Interaction of biomimetic apatite colloidal nanoparticles with human blood components, *Colloids and Surfaces B: Biointerfaces* 145 (2016) 87--94.
- [19] C. Drouet, A. Al-Kattan, M. Choimet, A. Tourrette, V. Santran, J. Dexpert-Ghys, B. Pipy, F. Brouillet, M. Tourbin, Biomimetic Apatite-Based Functional Nanoparticles as Promising Newcomers

- in Nanomedicine: Overview of 10 Years of Initiatory Research, *Journal of General Practice and Medical Diagnosis* (2015) 1-9.
- [20] A. Al-Kattan, V. Santran, P. Dufour, J. Dexpert-Ghys, C. Drouet, Novel contributions on luminescent apatite-based colloids intended for medical imaging, *Journal of Biomaterials Applications* 28(5) (2014) 697-707.
- [21] A. Al-Kattan, S. Girod-Fullana, C. Charvillat, H. Ternet-Fontebasso, P. Dufour, J. Dexpert-Ghys, V. Santran, J. Bordre, B. Pipy, J. Bernad, C. Drouet, Biomimetic nanocrystalline apatites: Emerging perspectives in cancer diagnosis and treatment, *International Journal of Pharmaceutics* 423(1) (2012) 26-36.
- [22] T. Welzel, I. Radtke, W. Meyer-Zaika, R. Heumann, M. Epple, Transfection of cells with custom-made calcium phosphate nanoparticles coated with DNA, *Journal of Materials Chemistry* 14(14) (2004) 2213-2217.
- [23] A. Doat, M. Fanjul, F. Pellé, E. Hollande, A. Lebugle, Europium-doped bioapatite: A new photostable biological probe, internalizable by human cells, *Biomaterials* 24(19) (2003) 3365-3371.
- [24] A. Al-kattan, P. Dufour, C. Drouet, Purification of biomimetic apatite-based hybrid colloids intended for biomedical applications: A dialysis study, *Colloids and Surfaces B: Biointerfaces* 82(2) (2011) 378-384.
- [25] G. Spada, E. Gavini, M. Cossu, G. Rassu, A. Carta, P. Giunchedi, Evaluation of the effect of hydroxypropyl-beta-cyclodextrin on topical administration of milk thistle extract, *Carbohydr Polym* 92(1) (2013) 40-7.
- [26] S. Sarda, M. Iafisco, P. Pascaud-Mathieu, A. Adamiano, M. Montesi, S. Panseri, O. Marsan, C. Thouron, A. Dupret-Bories, A. Tampieri, C. Drouet, Interaction of Folic Acid with Nanocrystalline Apatites and Extension to Methotrexate (Antifolate) in View of Anticancer Applications, *Langmuir* 34(40) (2018) 12036-12048.
- [27] A. Haq, B. Goodyear, D. Ameen, V. Joshi, B. Michniak-Kohn, Strat-M<sup>®</sup> synthetic membrane: Permeability comparison to human cadaver skin, *International Journal of Pharmaceutics* 547(1) (2018) 432-437.
- [28] M. Cossu, G. Rassu, E. Gavini, P. Giunchedi, Permeation test cell, Italy, 2019.
- [29] A. Al-Kattan, P. Dufour, J. Dexpert-Ghys, C. Drouet, Preparation and physicochemical characteristics of luminescent apatite-based colloids, *Journal of Physical Chemistry C* 114(7) (2010) 2918-2924.
- [30] C. Rey, C. Combes, C. Drouet, S. Cazalbou, D. Grossin, F. Brouillet, S. Sarda, Surface properties of biomimetic nanocrystalline apatites; applications in biomaterials, *Progress in Crystal Growth and Characterization of Materials* 60(3-4) (2014) 63--73.
- [31] P. Scherrer, Bestimmung der Größe und der inneren Struktur von Kolloidteilchen mittels Röntgenstrahlen, *Nachrichten von der Gesellschaft der Wissenschaften zu Göttingen, Mathematisch-Physikalische Klasse* (1918) 98-100.
- [32] N. Vandecandelaere, C. Rey, C. Drouet, Biomimetic apatite-based biomaterials : on the critical impact of synthesis and post-synthesis parameters, *J. Mater. Sci: Mater. Med* 23 (2012) 2593-2606.
- [33] C. Drouet, Apatite formation: why it may not work as planned, and how to conclusively identify apatite compounds, *BioMed research international* 2013 (2013) 490946-490946.
- [34] G.E. Flaten, Z. Palac, A. Engesland, J. Filipovic-Grcic, Z. Vanic, N. Skalko-Basnet, In vitro skin models as a tool in optimization of drug formulation, *Eur J Pharm Sci* 75 (2015) 10-24.
- [35] T. Uchida, W.R. Kadhum, S. Kanai, H. Todo, T. Oshizaka, K. Sugibayashi, Prediction of skin permeation by chemical compounds using the artificial membrane, Strat-M, *Eur J Pharm Sci* 67 (2015) 113-118.
- [36] G. Rassu, E. Soddu, M. Cossu, A. Brundu, G. Cerri, N. Marchetti, L. Ferraro, R.F. Regan, P. Giunchedi, E. Gavini, A. Dalpiaz, Solid microparticles based on chitosan or methyl-beta-cyclodextrin: a first formulative approach to increase the nose-to-brain transport of deferoxamine mesylate, *J Control Release* 201 (2015) 68-77.

- [37] R.W. McClain, B.A. Yentzer, S.R. Feldman, Comparison of skin concentrations following topical versus oral corticosteroid treatment: reconsidering the treatment of common inflammatory dermatoses, *J Drugs Dermatol* 8(12) (2009) 1076-9.
- [38] U. Nygaard, M. Deleuran, C. Vestergaard, Emerging Treatment Options in Atopic Dermatitis: Topical Therapies, *Dermatology* 233(5) (2017) 333-343.
- [39] C.R. Bruner, S.R. Feldman, M. Ventrapragada, A.B. Fleischer, Jr., A systematic review of adverse effects associated with topical treatments for psoriasis, *Dermatol Online J* 9(1) (2003) 2.
- [40] E. Makrantonaki, R. Ganceviciene, C. Zouboulis, An update on the role of the sebaceous gland in the pathogenesis of acne, *Dermato-endocrinology* 3(1) (2011) 41-49.
- [41] C. Rey, C. Combes, C. Drouet, M.J. Glimcher, Bone mineral: update on chemical composition and structure, *Osteoporosis International* 20(6) (2009) 1013-1021.
- [42] C. Drouet, M. Choimet, M. Simon, G. Deves, P. Barberet, H. Sez nec, G. Rassu, O. Marsan, A. Tourette, Colloidal apatite particles: a multifunctional platform in (nano)medicine, *Juniper Online Journal Material science* 6(1) (2020) article 555676.
- [43] E. Abd, S.A. Yousef, M.N. Pastore, K. Telaprolu, Y.H. Mohammed, S. Namjoshi, J.E. Grice, M.S. Roberts, Skin models for the testing of transdermal drugs, *Clinical pharmacology : advances and applications* 8 (2016) 163-176.